Europe PMC Funders Group
Author Manuscript
*Nat Catal*. Author manuscript; available in PMC 2020 March 09.

Published in final edited form as:
*Nat Catal*. 2019 October ; 2(10): 864–872. doi:10.1038/s41929-019-0333-4.

# Cancer-derived exosomes loaded with ultrathin palladium nanosheets for targeted bioorthogonal catalysis

**María Sancho-Albero**[#1,2], **Belén Rubio-Ruiz**[#3,±], **Ana M. Pérez-López**[#3], **Víctor Sebastián**[#1,2], **Pilar Martín-Duque**[4], **Manuel Arruebo**[1,2], **Jesús Santamaría**[1,2,*], **Asier Unciti-Broceta**[3,*]

[1]Department of Chemical Engineering, Aragon Institute of Nanoscience (INA), University of Zaragoza, Campus Río Ebro-Edificio I+D, c/Poeta Mariano Esquillor s/n, 50018 Zaragoza, Spain

[2]Networking Research Center on Bioengineering, Biomaterials and Nanomedicine (CIBER-BBN), 28029 Madrid, Spain

[3]Cancer Research UK Edinburgh Centre, MRC Institute of Genetics & Molecular Medicine, University of Edinburgh, Crewe Road South, Edinburgh EH4 2XR, UK

[4]Instituto Aragonés de Ciencias de la Salud//Fundación Araid//IIS Aragón. Centro de Investigaciones Biomédicas de Aragón, Avda San Juan Bosco 13, 50009 Zaragoza, Spain

[#] These authors contributed equally to this work.

## Abstract

The transformational impact of bioorthogonal chemistries has inspired new strategies for the *in vivo* synthesis of bioactive agents through non-natural means. Among these, palladium (Pd) catalysts have played a prominent role in the growing subfield of bioorthogonal catalysis by producing xenobiotics and uncaging biomolecules in living systems. However, delivering catalysts selectively to specific cell types still lags behind catalyst development. Here we have developed a bio-artificial device consisting of cancer-derived exosomes loaded with Pd catalysts by a method that enables the controlled assembly of Pd nanosheets directly inside the vesicles. This hybrid system mediates Pd-triggered dealkylation reactions *in vitro* and inside cells and displays preferential tropism for their progenitor cells. The use of Trojan exosomes to deliver abiotic catalysts into designated cancer cells creates the opportunity for a new targeted therapy modality: exosome-directed catalyst prodrug therapy, whose first steps are presented herein with the cell-specific release of the anticancer drug panobinostat.

---

Users may view, print, copy, and download text and data-mine the content in such documents, for the purposes of academic research, subject always to the full Conditions of use:http://www.nature.com/authors/editorial_policies/license.html#terms

**Correspondence and requests of materials** should be addressed to Jesús Santamaría (jesus.santamaria@unizar.es) and Asier Unciti-Broceta (Asier.Unciti-Broceta@igmm.ed.ac.uk).
[±] **Current address of B.R.-R:** Pfizer-University of Granada-Andalusian Regional Government Centre for Genomics and Oncological Research (GENYO) and Department of Medicinal & Organic Chemistry, Faculty of Pharmacy, University of Granada, Campus de Cartuja s/n, 18071 Granada, Spain.

**Competing Interests**
The authors declare that compound **4** is protected under patent application PCT/GB2017/051379.

**Author Contributions**
M.S.-A., B.R.-R., A.M.P.-L. and V.S. prepared and characterised the materials, planned and performed the experiments, analysed the data and wrote the Methods; V.S., P.M.-D. and M.A. planned and supervised the research, analysed the data and contributed to the manuscript writing; J.S. and A.U.-B. designed, coordinated and supervised the research, analysed the data and wrote the paper. All the authors checked the manuscript.

Europe PMC Funders Author Manuscripts

Europe PMC Funders Author Manuscripts

Europe PMC Funders Author Manuscripts

Europe PMC Funders Author Manuscripts

## Introduction

In recent years, transition metals conventionally confined to the chemistry lab (e.g. Pd, Ru, Au) have been shuttled into living cells, tissues and animals in pursuit of tools capable of catalysing first-in-life reactions.[1–31] From organometallic complexes,[1–13] artificial metalloenzymes[14–16] and metal-loaded nanocarriers[17–24] to larger-than-cells implantable devices,[25–31] a selected number of agents have demonstrated catalytic activity and maintained their functional compatibility with the biological milieu. Although the development of effective intracellular catalysts based on abiotic metals remains challenging, various examples reported in the literature have tested the feasibility of this concept.[4–9,16–24,32] One of the most exciting opportunities of this active field of research is, however, still in its infancy: the development of devices that not only display bioorthogonal catalytic activity but are also precisely delivered to specific anatomical locations, e.g. inside tumors.[21,23,30] First attempts to achieve this have explored physical (EPR effect, magnetism)[21,23] and surgical[30] approaches, but intercellular trafficking pathways have not yet been investigated. In principle, natural cell-specific delivery vectors such as exosomes[33] could be ideally suited to carry miniaturized catalytic reactors to individual cancerous cells.

Exosomes are membrane-enclosed vesicles released by cells to the extracellular space to mediate intercellular exchange of biomolecules and thereby regulate a variety of physiological functions.[33–35] The biochemical composition of the exosomal membrane is reflective of the donor cell, thus conferring on the exosomes a preferential tropism for cells that are parented to their cell of origin.[34,35] In the tumour microenvironment, exosomes are believed to play a fundamental role in the communication between cancer cells to orchestrate cancer progression, invasion, angiogenesis and immune regulation.[35–37] Thanks to their long circulating half-life, small size, low immunogenicity and ability to preferentially target particular cell types, exosomes exhibit ideal characteristics as vectors to deliver a therapeutic cargo (such as drugs, biomolecules or hyperthermia-capable nanoparticles) to specific cells.[38,39] However, introducing large molecules or nanoparticles inside exosomes is challenging because the methods often used (e.g. electroporation, sonication, etc.) can disrupt the exosomal membrane and compromise their targeting ability.

Here, motivated by the possibility of using exosomes as Trojan horses,[34,38–41] we aimed to hijack this ancient intercellular communication system to protect and deliver a catalytic cargo into a specific type of cancer cells. To implement this strategy, a mild chemical methodology was first developed to enable the controlled assembly of Pd nanostructures directly inside cancer cell-derived exosomes without compromising their integrity and functionality. The resulting bioartificial vesicles (**Pd-Exo**) are highly catalytic under physiological conditions, capable of preferentially delivering their catalytic cargo to their target cells and activate an anticancer prodrug inside them by Pd-mediated dealkylation. The concept of using exosome-directed catalyst delivery into designated cell types to mediate bioorthogonal processes in the inner cell space opens up a plethora of possibilities in the fields of chemical biology and biomedicine.

Europe PMC Funders Author Manuscripts

Europe PMC Funders Author Manuscripts

# Results

## Design, fabrication and characterization of Pd-Exo

The use of exosomes as drug delivery carriers has attracted increasing attention from academics and industry in recent years.[42] Various methods have been developed to ship a diverse range of therapeutic agents inside exosomes, including small molecule drugs, proteins, RNA molecules, and more complex cargoes such as modified viruses and gene-editing tools.[43–50] Rather than loading exosomes with a limited amount of a bioactive agent, we rationalized that the incorporation of transition metal-based catalysts into such a targeted delivery system could be used to build a deliverable nanoreactor able to direct a bioorthogonal catalytic payload towards cancer cells and facilitate amplified production of therapeutic agents directly at the cancer site. The first challenge was to develop a method that allows loading a metal of choice into these vesicles without affecting the exosome targeting properties and preserves the metal's catalytic activity, since current biophysical techniques for loading exosomes with metallic nanostructures[51–55] can induce detrimental defects on the integrity of the exosome membrane.[56,57]

Encouraged by prior success on the controlled growth of Pd nanosheets using carbon monoxide (CO) as a gaseous reducing agent under wet conditions,[58,59] a chemical methodology was investigated to generate Pd nanostructures directly inside exosomes. Figure 1A illustrates the stepwise production of **Pd-Exo$^{A549}$** (see full procedure in the Methods). After purification by ultracentrifugation from non-small cell lung carcinoma (NSCLC) A549 cell culture (see Suppl. Fig. 1), cancer-derived exosomes **Exo$^{A549}$** were incubated with $K_2PdCl_4$ (water soluble $Pd^{2+}$ reagent) in PBS at physiological conditions for 12 h. This was then followed by a second ultracentrifugation step (to remove extracellular $Pd^{2+}$ species) and 40-min treatment under a CO atmosphere (6 bar) and gentle stirring at low temperature (30 °C, to prevent protein denaturation) to mediate the *in situ* reduction of $Pd^{2+}$ to $Pd^0$ and self-assembly into stable Pd nanostructures. Procedural conditions (temperature, incubation times, CO pressure, etc.) were optimized for each step of the protocol to enhance the diffusion of $Pd^{2+}$ species and reductant gas through the exosome membrane, promoting Pd nanoparticle formation without causing functional defects to the exosomes. The choice of a mild antioxidant such as CO was addressed to minimize side reactions, since most reductants capable of reducing $Pd^{2+}$ species can potentially react with functional groups present in most biomolecules, including proteins and lipids of the exosome membrane.

Exosomes were characterized before and after treatment by different procedures, including physicochemical (transmission electron microscopy (TEM), cryo-TEM, high-resolution scanning TEM-high angle annular dark field (HRSTEM-HAADF), inductively coupled plasma mass spectrometry (ICP-MS), X-ray spectroscopy, and zeta potential nanoparticle tracking analysis (NTA)) as well as biological (Western Blot assays against different protein markers, total protein content) techniques. Rounded vesicles with an average diameter of 100-140 nm were observed from both samples, whereas dark nanostructures (Pd) with laminar shape were only visible inside **Pd-Exo$^{A549}$** (Figure 1B). Importantly, all **Pd-Exo$^{A549}$** contained such nanostructures and minimal alterations were observed in the size and morphology of the vesicles. Due to the benefits of vesicle cryopreservation, cryo-TEM

Europe PMC Funders Author Manuscripts

Europe PMC Funders Author Manuscripts

permitted visualization of the native spherical morphology of **Pd-Exo$^{A549}$** and identified the presence of numerous Pd-nanosheets that can be observed mainly clustered around the exosomal membrane. HRSTEM-HAADF was then employed to study the crystallinity of the Pd nanosheets inside exosomes (Figure 1D,E), revealing lattice fringes with d-spacing of 0.23 nm that match with metallic Pd (1 1 1)-surfaces.[60] The Fast Fourier Transform spectrum generated from this image (see inset of Fig 1E) corroborated this observation. This agrees with the expected dual role of CO as an electron donor to reduce $Pd^{2+}$ ions to $Pd^0$ atoms and as a capping agent to control the confined growth of Pd structures into a planar shape due to its preferential adsorption to basal {111}.[58] High resolution imaging showed the Pd nanostructures displayed an oriented 2D configuration (nanosheets) with a thickness of approximately 1.4 nm. The amount of Pd inside the vesicles was quantified by ICP-MS (ElanDRC-e, PerkinElmer) and normalized to the total protein amount of **Pd-Exo$^{A549}$**, providing an average Pd content of 0.64 μg of Pd / μg of **Pd-Exo$^{A549}$** protein. UV-VIS spectral analysis showed a maximal absorbance peak in the near infrared range (Supp. Fig. 3), which is characteristic of Pd nanosheets[58], while energy-dispersive X-ray spectroscopy analysis (Suppl. Fig. 4) and X-ray photoelectron spectroscopy (XPS, see Suppl. Fig. 5)[24] confirmed the presence of $Pd^0$ inside the exosomes. Analysis of the atomic environment for N 1s detected no changes between **Exo$^{A549}$** and **Pd-Exo$^{A549}$**, suggesting that the employed methodology does not alter protein composition.

To further study if membrane proteins had been altered during the chemical procedure, the presence of exosome-specific antigens CD9, CD63, CD81 and ALIX were characterized by western blot. As shown in Figure 1F, similar protein levels were observed before and after Pd loading, indicating that the mild reductive conditions employed to reduce $Pd^{2+}$ species do not degrade membrane proteins. Under native (non-denaturing) conditions, same bands were observed for both samples, but their migration rate showed clear differences (see Suppl. Fig. 6). The protein bands from **Pd-Exo$^{A549}$** migrated at a reduced rate and slightly towards the left, indicating a change in charge and mass. This artefact may be consequence of the **Pd-Exo$^{A549}$** lysing step during sample processing and attributed to coordination with free Pd species.[61] The low impact of the process to the protein composition of the exosomes is further supported by the XPS data (Suppl. Fig. 6) and the zeta potential analysis (Suppl. Fig. 7). Also, bicinchoninic acid assay showed that the CO treatment did not affect total exosomal protein content. Protein concentrations of 101.45 and 102.95 μg/mL were respectively obtained for **Exo$^{A549}$** and CO-treated **Exo$^{A549}$**.

The stability of this hybrid system was studied by analysis of particle size and zeta potential of **Exo$^{A549}$** and **Pd-Exo$^{A549}$** at different time points using a Nanosight NS500 (Malvern Instruments Ltd, UK) and a Zeta Plus (Brookhaven Instruments Corp., USA), respectively. As shown in Suppl. Fig. 7, average particle diameters of the exosomes before and after NP generation were equivalent (146.5 and 155 nm, respectively) and the size and zeta potential of **Pd-Exo$^{A549}$** remain relatively stable after 72 h at room temperature, indicating that Pd-loaded exosomes are sufficiently stable to perform reproducible *in vitro* and cell-based studies.

Europe PMC Funders Author Manuscripts

Europe PMC Funders Author Manuscripts

## Pd-Exo$^{A549}$ as catalytic nanoreactors

The catalytic properties of **Pd-Exo**$^{\mathbf{A549}}$ were evaluated with the Pd-sensitive off-on sensor **1**, which was designed to release the membrane-permeant red-fluorescent dye resorufin (**2**) upon a single *O*-depropargylation reaction (see Figure 2A). The lipophilicity of both **1** and **2** facilitates back-and-forth diffusion across the exosome membrane before and after activation, thus facilitating reaction monitoring by fluorometric analysis of the reaction medium. Compound **1** was synthesized by reacting **2** with propargyl bromide and DBU in DMF at room temperature. As shown in Suppl. Fig 8, **1** shows negligible fluorescence emission under white LED excitation (>200-fold difference compared to that of dye **2** at 590 nm), a consequence of blocking the electronic conjugation of the system by alkylation of the phenolic OH.

**Pd-Exo**$^{\mathbf{A549}}$ were incubated at different concentrations (0.12, 0.16, 0.2 and 0.4 µg/100µL) with non-fluorescent compound **1** (100 µM) in PBS and 37 °C for 16 h. Note that, to be able to study and compare the activity of vesicles loaded or not with Pd, the concentration values used in the experiments are expressed as µg of exosome protein /100 µL. The fluorescence intensity of the samples was measured with a spectrofluorometer (Ex/Em: 540/590 nm) and values compared to that of **2** at 100 µM (= 100% conversion). Incubation of sensor **1** (100 µM) alone or in the presence of **Exo**$^{\mathbf{A549}}$ (0.2 µg / 100µL) were used as negative controls. Treatment of **1** with **Pd-Exo**$^{\mathbf{A549}}$ resulted in a dramatic increase of fluorescent emission, with the top concentrations of 0.2 and 0.4 µg / 100µL yielding near to complete conversion (>97% yield after 16 h, see Figure 2B). In contrast, sensor **1** was stable on its own and in the presence of **Exo**$^{\mathbf{A549}}$ (no fluorescence detected). Time lapse imaging of the reaction illustrates the fast conversion rate of non-fluorescent **1** into highly red fluorescent **2** in the presence of Pd-loaded exosomes (see Supp. Video 1).

To further study the kinetics of the process, three concentrations of substrate **1** (25, 50 and 100 µM) were treated with **Pd-Exo**$^{\mathbf{A549}}$ (0.2 µg/100 µL) at the same conditions and the formation of dye **2** monitored by fluorometry at different timepoints. As shown in Figure 2C, the rate of product formation followed a classical Michaelis Menten growth curve and all reactions were completed before 24 h. Kinetic parameters were calculated by plotting the natural log of the concentration of substrate ([**1**]) versus time (Suppl. Fig. 9), displaying pseudo first-order kinetics with a $K = 0.1228 \pm 0.0049\ s^{-1}$ and half-life of 5.64 h at the range of concentrations used. These results agree with the *O*-depropargylation rate found for previously-reported Pd-based heterogeneous catalysts.[25–30] The reusability of **Pd-Exo**$^{\mathbf{A549}}$ was then tested by recycling (centrifugation) the vesicles after reaction with **1**, followed by re-treatment with **1**. Repetition of this process 3 times verified the recyclability of these catalytic vesicles (Supp. Fig. 10), although a moderate reduction of activity (45% and 20% reduction yield in cycles 2 and 3, respectively) was observed after each cycle, which we attribute to a loss of material due to incomplete recovery by the centrifugation process.

## Pd-Exo$^{A549}$ biocompatibility and intracellular entry

The tolerability of human cells to exposure to Pd-loaded exosomes was determined by incubating increasing quantities of **Pd-Exo**$^{\mathbf{A549}}$ with lung cancer A549 cells for 5 d. Cell viability assays showed that **Pd-Exo**$^{\mathbf{A549}}$ induce minimal effect on cell proliferation even at the top dose of 0.6 μg / 100μL (see Supp. Fig. 11).

Next, the internalization of **Pd-Exo**$^{\mathbf{A549}}$ into their parental cells A549 was studied by confocal microscopy in search for the optimal incubation time to perform intracellular catalytic experiments. After treating A549 cells with **Pd-Exo**$^{\mathbf{A549}}$ under standard cell culture conditions, cells were fixed and labelled with phaloidin-488 (actin fibres) and Draq5 (nuclei). Due to the inherent reflective optical properties of the Pd nanosheets, clusters of **Pd-Exo**$^{\mathbf{A549}}$ were directly observed by reflection of the incident light in the confocal microscope at 488/490 nm excitation/emission wavelengths (identified in Figure 3 as red dots). Representative images from A549 cells after treatment with **Pd-Exo**$^{\mathbf{A549}}$ for 1, 2, 4 and 6 h are shown in Figure 3 (see study at 24 h in Suppl. Fig. 12). Quantitative analysis of the red fluorescent signal confirmed that the highest cytoplasmic presence of Pd-loaded vesicles was reached after 6 h incubation of cells with **Pd-Exo**$^{\mathbf{A549}}$ (Suppl. Fig. 13). Z-stack sections of the images at 6 h confirmed the intracellular localization of **Pd-Exo**$^{\mathbf{A549}}$ aggregates (Figure 3), while co-localization studies revealed that the majority of Pd-nanosheets were not in lysosomal compartments at that time point (Suppl. Fig. 14).

## Targeted intracellular prodrug activation mediated by Pd-Exo$^{A549}$

The pan-histone deacetylase (HDAC) inhibitor panobinostat (**3**) received clinical approval to treat multiple myeloma in 2015,[62] and is currently in clinical trials for the treatment of a variety of cancers including NSCLC. Despite its broad activity against many cancer types, dose-limiting systemic toxicities including diarrhoea, cardiac ischemic events, arrhythmias and myelosuppression, limit the use of panobinostat and other HDAC inhibitors against solid tumours. Selective delivery and localized activation of this class of epigenetic targeting drugs at cancer sites have been proposed to enhance their clinical tolerability and antitumor efficacy, with different prodrug strategies for medically-used vorinostat and belinostat being recently showcased in the literature.[63,64] However, prodrugs of **3** have not yet been reported, perhaps due to its higher structural complexity.

At this point of the investigation, **Pd-Exo**$^{\mathbf{A549}}$ had shown to be catalytic under physiological conditions, harmless to cells and capable of entering A549 cells. To further challenge the multifunctional capacities of the nanodevices, it was essential to determine if **Pd-Exo**$^{\mathbf{A549}}$ were also able to mediate the bioorthogonal uncaging of a bioactive substance inside their target cells. To test this, a Palladium-activatable prodrug of **3** was developed (see Figure 4A). Given the essential role of the Zn-chelating hydroxamate group of **3** in its cytotoxic mode of action,[64] the *O*-alkyl hydroxamate derivative **4** was designed to reduce its capacity to inhibit HDACs while, at the same time, making it sensitive to Pd chemistry.

Direct attempts to alkylate the OH group of **3** with *p*-(propargyloxy)benzyl bromide[64] were unsuccessful due the presence of various nucleophilic groups in the molecule. Consequently, compound **4** was prepared by total synthesis following the scheme summarized in Figure 4B. Briefly, *p*-(propargyloxy)benzyl bromide (**5**) was reacted with *N*-hydroxyphthalimide in the presence of HNa to afford intermediate **6**, which was converted into hydroxylamine **7** by hydrazinolysis. β-Substituted-acrylic acid **9** was prepared by reductive amination of 3-(4-

formyl-phenyl)-acrylic acid methyl ester with 2-methyltryptamine (**8**)[65] followed by basic hydrolysis. Carbodiimide-mediated coupling of **7** and **9** resulted in the generation of prodrug **4** in moderate yield.

To evaluate the efficiency of the masking strategy, the antiproliferative properties of prodrug **4** and unmodified drug **3** were assessed against NSCLC A549 and glioblastoma U87 cells. Cells were treated for 5 d with compounds at concentrations ranging from 0.003 to 100 μM and cell viability determined with the PrestoBlue reagent. Comparison between the dose response curves of **3** and **4** evidenced that the alkylation of the hydroxamate group leads to a significant reduction of the bioactivity of the compound in both cell lines (see Suppl. Fig. 15).

Next, a cell-based assay was performed to determine if the devices have preferential tropism for their progenitor cells[66] by comparing their capacity to mediate bioorthogonal uncaging reactions in different cell types. Two cell lines were used for the experiment: the parental cancer cells A549 (target cells) and unparented glioblastoma cells U87 (non-target cells). To maximise cell entry, A549 and U87 cells were incubated with **Pd-Exo$^{\mathbf{A549}}$** for 6 h at 0.4 or 0.53 μg / 100μL, respectively. Note that higher **Pd-Exo$^{\mathbf{A549}}$** concentration was used for U87 cells to normalise the quantity of vesicles per number of seeded cells. After several washing steps to remove non-internalised vesicles, cells were treated with prodrug **4** for 5 d (0.2 μM; activation assay), aiming to observe a reduction in cell viability resulting from the bioorthogonal release of cytotoxic **3** in cells containing catalytically-active **Pd-Exo$^{\mathbf{A549}}$**. Cells separately treated with **4** (0.2 μM) or **Pd-Exo$^{\mathbf{A549}}$** were used as negative controls, and treatment with **3** (0.2 μM) used as positive control. As observed in Figure 4C, A549 cells sequentially treated with **Pd-Exo$^{\mathbf{A549}}$** and **4** exhibited significantly lower cell viability than the negative controls, evidence of the generation of cytotoxic levels of **3** inside cells and, therefore, of the presence of catalytically-active **Pd-Exo$^{\mathbf{A549}}$**. Additional negative controls further confirmed that the observed cytotoxic activity was driven by Pd mediated drug uncaging (Suppl. Fig. 16 and 17). In contrast, no effect was observed on the viability of U87 cells after the same treatment, indicating that the lower uptake or the reduced catalytic activity of **Pd-Exo$^{\mathbf{A549}}$** in U87 cells results in insufficient intracellular production of drug **3**.

To study if the reverse situation was also true, i.e. superior uptake of catalytically-active **Pd-Exo$^{\mathbf{U87}}$** by U87 cells relative to A549 cells leads to higher prodrug-into-drug conversion levels and cell death, **Pd-Exo$^{\mathbf{U87}}$** were generated from U87 cells following the methodology described before. After ICP-MS analysis and testing their catalytic properties in vitro (see Suppl. Fig. 19), A549 and U87 cells were sequentially treated with **Pd-Exo$^{\mathbf{U87}}$** and **4** using the same conditions and controls above described, and cell viability measured at day 5. As shown in Fig 4D, results followed the opposite trend to those found with **Pd-Exo$^{\mathbf{A549}}$**, further supporting that the preferential tropism of exosomes for their cancer cells of origin is important to deliver sufficient Pd nanosheets into cells and produce bioactive concentrations of drug **3**.

Additionally, this study was carried out in a third cell line: the monocyte/macrophage-like cell line RAW 264.7. These phagocytic cells were independently treated with **Pd-Exo$^{\mathbf{A549}}$** or **Pd-Exo$^{\mathbf{U87}}$**, followed by treatment with **4**. Suppl. Fig. 20 shows that both **Pd-Exo** / **4**

Europe PMC Funders Author Manuscripts

Europe PMC Funders Author Manuscripts

Europe PMC Funders Author Manuscripts

Europe PMC Funders Author Manuscripts

combinations were capable of reducing cell proliferation in this cell line, evidence of *in situ* drug **3** synthesis, although at lower levels than those achieved in their cell of origin, even if RAW 264.7 cells are much more sensitive to **3**. It is important to note that while the higher **Pd-Exo** internalisation levels would be consistent with the results observed, they are not the only factor in play. Thus, differences in intracellular trafficking routes could also have a significant effect in the exosome-mediated delivery of catalytically-active Pd nanostructures into progenitor cells.

Last, *in situ* production of **3** was further confirmed by studying intracellular target displacement of coumarin–SAHA, a blue-emitting fluorescent inhibitor of HDAC proteins whose fluorescent properties are quenched when bound to their targets.[64] Displacement from their targets by other competitive inhibitor results in an increase of intracellular fluorescence intensity that can be measured by flow cytometry (λex/em = 405/450 nm) and thereby be used as evidence of *in situ* drug synthesis and target engagement. As shown in Suppl. Fig. 21, cells pre-treated with coumarin-SAHA and **Pd-Exo**$^{\mathbf{A549}}$ followed by washing and treatment with prodrug **4** resulted in significantly higher fluorescent intensity than in the absence of **Pd-Exo**$^{\mathbf{A549}}$, further corroborating the intracellular generation of biologically-effective levels of **3** by Palladium chemistry.

## Conclusions

The nanoscale bio-hybrid system developed in this work brings together the targeting capabilities of exosomes, a robust intercellular trafficking pathway evolved in nature across millions of years, and the bioorthogonal concept developed by Bertozzi and others[67–69] in the last two decades. Cell-targeting catalytic devices can be generated from cancer-derived exosomes using a methodology based on CO-mediated reduction at low temperature to generate ultrathin Pd nanosheets directly inside the vesicles. The mildness of the protocol yielded catalytically active Pd nanostructures that maintained the targeting capabilities of the exosomes. This methodology can be considered —in its own right— as a bioorthogonal process suitable to load metallic structures into biological vesicles.

The development of Pd nanodevices that can perform uncaging chemistries inside cells require robust vectors able to enter cells with high efficacy and compatible with the complex intracellular environment (redox, pH, etc.). Herein we show that **Pd-Exo** not only display the capacity of entering the cancer cells from where they originated and perform bioorthogonal uncaging reactions, but also the ability to discriminate over other cell types. The intracellular catalytic properties of **Pd-Exo**$^{\mathbf{A549}}$ were demonstrated by the *in situ* activation of the anticancer drug panobinostat in lung cancer A549 cells, but not in U87 (a glioma cell line), indicating preferential tropism for their progenitor cells. Opposite results were observed in the reverse situation, i.e. Pd-loaded exosomes originated from U87 cells displayed superior drug-mediated cytotoxic effect in U87 cells than in A549 cells. This proof-of-concept study illustrates the therapeutic potential of combining exosome-mediated delivery of catalysts and bioorthogonal uncaging chemistries to activate bioactive substances in a spatiotemporal selective manner.

Europe PMC Funders Author Manuscripts

Europe PMC Funders Author Manuscripts

# Methods

## $Exo^{A549}$ purification and characterization

A549 cells (kind gift from Dr S. Wilkinson; ATTC, CCL-185) or glioma U87 cells (a kind gift from Dr N. Gammoh; ATTC, HTB-14) were cultured in Dulbecco's modified Eagle's medium (DMEM) supplemented with 10 % fetal bovine serum (FBS), 1 % penicillin/ streptomycin and 1 % amphotericin, under normoxic conditions. Neither A549 nor U87 cell lines are included in the register of misidentified cell lines (source: ICLAC database v9, updated on October 2018). Cells were checked for mycoplasma before use. Ultracentrifuged serum (Ultracen medium, 100,000 g, 8 h, 4 ºC) was employed to guarantee exosomes free medium. **Exo** were collected and purified by successive ultracentrifugation cycles from supernatants of cell culture at confluency (see detailed protocol in the Supplementary Methods).

## Preparation of Pd-Exo

The purified exosome fraction was then dispersed in a PBS solution and treated with $K_2PdCl_4$ (0.06 mM) at 40 °C for 12 h to maximize the internalization of $Pd^{2+}$ ions. The mixture was subsequently ultracentrifuged at 35,000 g and 4ºC for 2 h to discard non-internalized Pd species and avoid contamination with extra-exosomal metal nanoparticles during the reduction step. **$Pd^{2+}$-Exo** were resuspended in PBS and treated for 40 min to a 6 bar CO atmosphere using a high-pressure Teflon lined autoclave under gentle stirring and 30 °C to reduction of $Pd^{2+}$ species into $Pd^0$. A light dark colour was immediately observed after CO treatment, inferring formation of Pd nanoparticles. After treatment, CO was desorbed with air to keep the resulting **Pd-Exo** in a neat environment.

## Characterization of $Exo^{A549}$ and Pd-$Exo^{A549}$

Phosphotungstic acid (3 %) was used as contrast agent to evaluate the morphology, size and shape of **$Exos^{A549}$** and **Pd-$Exo^{A549}$** by TEM operated at 200 kV with a LaB6 electron source fitted with a SuperTwin® objective lens allowing a point-to-point resolution of 2.4 Å. Analysis of the content specific exosome surface protein was performed by western blot. In brief, 10 μg of exosomes were lysed in RIPA buffer and the protein fraction precipitated with cold acetone (1:1 w/w) at -20 ºC for 2 h. The precipitated fraction was resuspended in Laemmly buffer and boiled at 90 ºC for 10 min. Subsequently, proteins were separated by 12 % SDS-polyacrylamide gel electrophoresis at 100 V for 2 h and transferred to a nitrocellulose membrane at 4 ºC for 4 h. Blots were blocked overnight with TBS-5% milk at 4 ºC and incubated with CD9; 1:2000 (Abcam, UK), CD63; 1:1000 (BD Bioscience, United States), CD81; 1:500 (Santa Cruz Biotechnology, United States) and ALIX; 1:1000 (Cell Signaling Technologies, United States) for 1.5 h. Membranes were washed 3 times with TBS-Tween (TTBS) followed by incubation of the secondary antibody (anti-HRP, Sigma Aldrich). Last, membranes were washed extensively and imagined by chemiluminescence.

Elemental analysis of **Pd-$Exo^{A549}$** was assessed with an EDS (EDAX) detector which allows performing EDS experiments in the scanning mode (FEI Inspect F30). The amount of Pd inside the vesicles was quantified by ICP-MS (ElanDRC-e, PerkinElmer) and normalized to the total protein amount of **Pd-$Exo^{A549}$**. For that, samples were digested with 10 % Aqua

Europe PMC Funders Author Manuscripts

Europe PMC Funders Author Manuscripts

regia ($HNO_3$ + 3HCl) in 1.5 mL of distilled water. Digestion was performed at rt for 1 h. Calibrations were carried out using Pd standards in 10 % Aqua regia ranging from 0 to 10 ppm. Characterization of the absorbance properties of **Pd-Exo$^{A549}$** was determined by UV-VIS spectroscopy (Jasco V670) to identify the characteristic plasmon at the NIR range of Pd nanosheets. For Cryo-TEM imaging, the grid preparation of cryogenically immobilized **Pd-Exo$^{A549}$** samples required an extremely rapid sample freezing to achieve a vitreous state. A thin film vitrified specimen was prepared with Vitrobot (FEI) in melting ethane. Afterwards, the sample holder with the specimen grid was maintained under cryogenic conditions with liquid nitrogen. Cryo-TEM observations were carried using a T20-FEI microscope with a LaB6 electron source fitted with a SuperTwin® objective lens allowing a point-to-point resolution of 2.4 Å. Total protein amount of native **Exo$^{A549}$** and **Exo$^{A549}$** treated with CO was quantified by Pierce BCA protein assay (Thermo Fisher Scientific, USA) following manufacturer instructions.

## Fluorogenic studies

0.6, 0.8, 1 and 2 μg of **Pd-Exo$^{A549}$** were added to a 500 μL solution of reagent **1** (100 μM) in PBS, to obtain a final concentration of 0.12, 0.16, 0.20 and 0.40 μg of **Pd-Exo$^{A549}$**/100 μL, respectively. The mixtures were shaken at 700 rpm and 37 °C in a Thermomixer, and reactions were monitored after 16 h using a PerkinElmer EnVision 2101 multilabel reader (Ex/Em: 540 /590 nm). Sensor **1** alone (100 μM) or in the presence of **Exo$^{A549}$** (1 μg of exosomes in 500 μL of PBS; 0.20 μg of **Exo$^{A549}$**/100 μL) were used as negative controls and fluorescent dye **2** at 100 μM as reference control. Reactions were done in triplicates and the conversion % calculated according to the reference control.

**Time-lapse imaging—**The **Pd-Exo$^{A549}$**–mediated activation of **1** into **2** was also visualized in real time by time lapse microscopy with a 20x objective (Ex/Em: 560/630 nm, Leica AF6000 LX, Germany), using non-fluorescent **1** alone as negative control and resorufin **2** alone as positive control. 0.5 μg of **Pd-Exo$^{A549}$** were added to a 20 μM solution of **1** in PBS (0.5 mL) in a 24-well plate and incubated for 24 h. Frames were taken every 15 min for 24 h in DIC mode and under fluorescence emission. Videos were created using Image*J* software.

**Reusability study—**After performing the reaction above described, **Pd-Exo$^{A549}$** were recovered by centrifugation (13,000 rpm, 30 min) and a fresh solution of **1** (100 μM) in PBS added to the recovered fraction of **Pd-Exo$^{A549}$**. The mixtures were shaken at 700 rpm and 37 °C in a Thermomixer, and reactions monitored after 16 h using a PerkinElmer EnVision 2101 multilabel reader (Ex/Em: 540 /590 nm). This cycle was repeated 3 times in total.

## Study of Pd-Exo$^{A549}$ biocompatibility

A549 cells were cultured in DMEM supplemented with 10 % of FBS and L-glutamine (2 mM) and maintained in a tissue culture incubator at 37 °C and 5% $CO_2$. Experiments were performed in DMEM supplemented with exosome-depleted FBS (Gibco™) and L-glutamine (2 mM). A549 cells were seeded in a 96-well plate format (at 1,500 cells / well) and incubated for 24 h before treatment. Each well was then replaced with a suspension of **Pd-Exo$^{A549}$** in culture media depleted of exosomes at 0.2, 0.4 and 0.6 μg per 100 μL and

Europe PMC Funders Author Manuscripts

incubated for 6 h. Cells were then washed with PBS buffer and fresh media added. After 5 d, PrestoBlue™ cell viability reagent (10 % v/v) was added to each well and the plate incubated for 90 min. Fluorescence emission was detected using a PerkinElmer EnVision 2101 multilabel reader (Ex / Em: 540 / 590 nm). Experiments were performed in triplicates.

### Confocal microscopy study of Pd-Exo$^{A549}$ cell internalization

A549 cells were seeded at a density of 1.5 x $10^4$ onto 20 mm cover slips (in a 24-well plate) and incubated under standard culture conditions for 24 h. 1 µg of **Pd-Exo$^{A549}$** was then added to each well and incubated for 1, 2, 4, 6 and 24 h. Cells were fixed with 4 % paraformaldehyde and stained with phalloidin-Alexa488 (Invitrogen) and Draq-5. Cells were imaged by confocal microscopy (Spectral Confocal Microscope Leica TCA SP2) with a 63x oil immersed N.A. 1.40 objective. Reflection of the incident light at 488/490 was used to directly visualized **Pd-Exo$^{A549}$**. Z-stack orthogonal projections were also carried out to enable visualization of exosomes inside cells cytosol.

### Cell viability study: 4 vs 3

Antiproliferative activity of **3** and **4** was compared by performing dose-response studies against A549 and U87 cells. Both cell lines were seeded in a 96-well plate format (at 1,500 cells / well for A549 and 2,000 cells / well for U87) and incubated for 24 h before treatment. Each well was then replaced with fresh media, containing compounds **3** and **4** (0.003-100 µM). Untreated cells were incubated with DMSO (0.1 % v/v). After 5 d of incubation, cell viability was determined as described above. All conditions were normalized to the untreated cells (100 %) and curves fitted using GraphPad Prism using a sigmoidal variable slope curve. Experiments were performed in triplicates.

### Intracellular prodrug activation study

A549 and U87 cells were seeded in a 96-well plate format (at 1,500 cells / well for A549 and 2,000 cells / well for U87) and incubated for 24 h before treatment. The corresponding wells were then replaced with a suspension of **Pd-Exo$^{A549}$** or **Pd-Exo$^{U87}$** in culture media depleted of exosomes (at 0.4 µg / 100 µL for A549 and 0.53 µg / 100 µL for U87, in order to normalize exosome quantity per number of seeded cell). After 6 h of incubation, these wells were washed with PBS buffer to remove extracellular vesicles and treated with fresh media containing either DMSO (0.1% v/v) or **4** (0.2 µM). Cells treated with **3** and **4** at 0.2 µM were used as positive and negative controls, respectively. After 5 d of treatment, cell viability was determined as described above. Experiments were performed in triplicates.

## Supplementary Material

Refer to Web version on PubMed Central for supplementary material.

## Acknowledgements

Financial support from EPSRC (Healthcare Technology Challenge Award EP/N021134/1) and the ERC Advanced Grant CADENCE (ERC-2016-ADG-742684) are gratefully acknowledged. We also thank Dr Silvia Irusta at the University of Zaragoza for performing XPS measurements. MSA thanks the Spanish Government for an FPU PhD research fellowship. BRR thanks the EC (H2020-MSCA-IF-2014-658833, ChemoBOOM). MA thanks the financial

Europe PMC Funders Author Manuscripts

Europe PMC Funders Author Manuscripts

support of the ERC Consolidator Grant program (ERC-2013-CoG-614715). PMD thanks AECC Fund and Refbio-Lactodermal for financial support.

## Data availability statement

The data that support the plots within this paper and other findings of this study are available from the corresponding author upon reasonable request.

## References

1. Streu C, Meggers E. Ruthenium-induced allylcarbamate cleavage in living cells. Angew Chem Int Ed. 2006; 45:5645–5648.
2. Li N, Lim RK, Edwardraja S, Lin Q. Copper-free sonogashira cross-coupling for functionalization of alkyne-encoded proteins in aqueous medium and in bacterial cells. J Am Chem Soc. 2011; 133:15316–15319. [PubMed: 21899368]
3. Spicer CD, Triemer T, Davis BG. Palladium-mediated cell-surface labeling. J Am Chem Soc. 2012; 134:800–803. [PubMed: 22175226]
4. Michel BW, Lippert AR, Chang CJ. A reaction-based fluorescent probe for selective imaging of carbon monoxide in living cells using a palladium-mediated carbonylation. J Am Chem Soc. 2012; 134:15668–15671. [PubMed: 22970765]
5. Yang M, Jia S, Zhang X, Chen P. Palladium-triggered deprotection chemistry for protein activation in living cells. Nat Chem. 2014; 6:352–361. [PubMed: 24651204]
6. Mascareñas JL, Sánchez MI, Penas C, Vázquez ME. Metal-catalyzed uncaging of DNA-binding agents in living cells. Chem Sci. 2014; 5:1901. [PubMed: 25632343]
7. Völker T, Dempwolff F, Graumann PL, Meggers E. Angew Chem Int Ed. 2014; 53:10536.
8. Wang J, et al. Chemical remodeling of cell-surface sialic acids through a palladium-triggered bioorthogonal elimination reaction. Angew Chem Int Ed. 2015; 54:5364–5368.
9. Tomás-Gamasa M, Martínez-Calvo M, Couceiro JR, Mascareñas JL. Transition metal catalysis in the mitochondria of living cells. Nat Commun. 2016; 7:12538. [PubMed: 27600651]
10. Tsubokura K, et al. In Vivo Gold Complex Catalysis within Live Mice. Angew Chem Int Ed. 2017; 56:3579–3584.
11. Destito P, Couceiro JR, Faustino H, López F, Mascareñas JL. Ruthenium-catalyzed azide-thioalkyne cycloadditions in aqueous media: a mild, orthogonal, and biocompatible chemical ligation. Angew Chem Int Ed. 2017; 56:10766–10770.
12. Vidal C, Tomás-Gamasa M, Destito P, López F, Mascareñas JL. Concurrent and orthogonal gold(I) and ruthenium(II) catalysis inside living cells. Nat Commun. 2018; 9:1913. [PubMed: 29765051]
13. Stenton BJ, Oliveira BL, Matos MJ, Sinatra L, Bernardes GJL. A thioether-directed palladium-cleavable linker for targeted bioorthogonal drug decaging. Chem Sci. 2018; 9:4185–4189. [PubMed: 29780549]
14. Chatterjee A, et al. An enantioselective artificial Suzukiase based on the biotin–streptavidin technology. Chem Sci. 2016; 7:673–677. [PubMed: 29896353]
15. Jeschek M, et al. Directed evolution of artificial metalloenzymes for in vivo metathesis. Nature. 2016; 537:661–665. [PubMed: 27571282]
16. Okamoto Y, et al. A cell-penetrating artificial metalloenzyme regulates a gene switch in a designer mammalian cell. Nat Commun. 2018; 9:1943. [PubMed: 29769518]
17. Yusop RM, Unciti-Broceta A, Johansson EMV, Sánchez-Martín RM, Bradley M. Palladium-mediated intracellular chemistry. Nat Chem. 2011; 3:239–243. [PubMed: 21336331]
18. Unciti-Broceta A, Johansson EMV, Yusop RM, Sánchez-Martín RM, Bradley M. Synthesis of polystyrene microspheres and functionalization with Pd(0) nanoparticles to perform bioorthogonal organometallic chemistry in living cells. Nat Protocols. 2012; 7:1207–1218. [PubMed: 22653159]
19. Tonga GY, Jeong Y, Duncan B, Mizuhara T, Mout R, et al. Supramolecular regulation of bioorthogonal catalysis in cells using nanoparticle-embedded transition metal catalysts. Nat Chem. 2015; 7:597–603. [PubMed: 26100809]

Europe PMC Funders Author Manuscripts

Europe PMC Funders Author Manuscripts

20. Miller MA, et al. Nano-palladium is a cellular catalyst for in vivo chemistry. Nat Commun. 2017; 8:15906–15919. [PubMed: 28699627]
21. Clavadetscher J, Indrigo E, Chankeshwara SV, Lilienkampf A, Bradley M. In-cell dual drug synthesis by cancer-targeting palladium catalysts. Angew Chem Int Ed. 2017; 56:6864–6868.
22. Hoop M, et al. Mobile magnetic nanocatalysts for bioorthogonal targeted cancer therapy. Adv Funct Mater. 2018; 28:1705920.
23. Liu Y, et al. Catalytically active single-chain polymeric nanoparticles: exploring their functions in complex biological media. J Am Chem Soc. 2018; 140:3423–3433. [PubMed: 29457449]
24. Wang F, Zhang Y, Du Z, Ren J, Qu X. Designed heterogeneous palladium catalysts for reversible light-controlled bioorthogonal catalysis in living cells. Nat Commun. 2018; 9:1209. [PubMed: 29572444]
25. Weiss JT, et al. Extracellular palladium-catalysed dealkylation of 5-fluoro-1-propargyl-uracil as a bioorthogonally activated prodrug approach. Nat Commun. 2014; 5:3277. [PubMed: 24522696]
26. Weiss JT, et al. Development and bioorthogonal activation of palladium-labile prodrugs of gemcitabine. J Med Chem. 2014; 57:5395–5404. [PubMed: 24867590]
27. Weiss JT, Carragher NO, Unciti-Broceta A. Palladium-mediated dealkylation of N-propargyl-floxuridine as a bioorthogonal oxygen-independent prodrug strategy. Sci Rep. 2015; 5:9329. [PubMed: 25788464]
28. Clavadetscher J, et al. Copper catalysis in living systems and in situ drug synthesis. Angew Chem Int Ed. 2016; 55:15662–15666.
29. Pérez-López AM, et al. Gold-triggered uncaging chemistry in living systems. Angew Chem Int Ed. 2017; 56:12548–12552.
30. Bray TL, et al. Bright insights into palladium-triggered local chemotherapy. Chem Sci. 2018; 9:7354–7361. [PubMed: 30542538]
31. Adam C, et al. Bioorthogonal uncaging of the active metabolite of irinotecan by palladium-functionalized microdevices. Chem Eur J. 2018; 24:16783–16790. [PubMed: 30187973]
32. Eda S, et al. Biocompatibility and therapeutic potential of glycosylated albumin artificial metalloenzymes. Nat Catal. 2019; doi: 10.1038/s41929-019-0317-4
33. Valadi H, et al. Exosome mediated transfer of mRNAs and microRNAs is a novel mechanism of genetic exchange between cells. Nat Cell Biol. 2007; 9:654–659. [PubMed: 17486113]
34. Gould SJ, Booth AM, Hildreth JE. The Trojan exosome hypothesis. Proc Natl Acad Sci USA. 2003; 100:10592–10597. [PubMed: 12947040]
35. Gourlay J, et al. The emergent role of exosomes in glioma. J Clin Neurosci. 2017; 35:13–23. [PubMed: 27771233]
36. Hornick NI, et al. AML suppresses hematopoiesis by releasing exosomes that contain microRNAs targeting c-MYB. Sci Signal. 2016; 9:ra88. [PubMed: 27601730]
37. Huan J, et al. Coordinate regulation of residual bone marrow function by paracrine trafficking of AML exosomes. Leukemia. 2015; 29:2285–2295. [PubMed: 26108689]
38. Alvarez-Erviti L, et al. Delivery of siRNA to the mouse brain by systemic injection of targeted exosomes. Nat Biotechnol. 2011; 29:341–345. [PubMed: 21423189]
39. Li X, et al. Exosomes in cancer: Small transporters with big functions. Cancer Lett. 2018; 435:55–65. [PubMed: 30071288]
40. Meckes DG Jr. Exosomal communication goes viral. J Virol. 2015; 89:5200–5203. [PubMed: 25740980]
41. Abrami L, et al. Hijacking multivesicular bodies enables long-term and exosome-mediated long-distance action of anthrax toxin. Cell Rep. 2013; 5:986–996. [PubMed: 24239351]
42. Cross R. Meet the exosome, the rising star in drug delivery. Chem Eng News. 2018; 96:22–23.
43. Zitvogel L, et al. Eradication of established murine tumors using a novel cell-free vaccine: dendritic cell-derived exosomes. Nat Med. 1998; 4:594–600. [PubMed: 9585234]
44. Munoz JL, et al. Delivery of functional anti-mir-9 by mesenchymal stem cell-derived exosomes to glioblastoma multiforme cells conferred chemosensitivity. Mol Ther Nucleic Acids. 2013; 2:e126. [PubMed: 24084846]

Europe PMC Funders Author Manuscripts

Europe PMC Funders Author Manuscripts

45. Smyth T, et al. Surface functionalization of exosomes using click chemistry. Bioconjug Chem. 2014; 25:1777–1784. [PubMed: 25220352]
46. Yang T, et al. Exosome delivered anticancer drugs across the blood-brain barrier for brain cancer therapy in Danio rerio. Pharm Res. 2015; 32:2003–2014. [PubMed: 25609010]
47. Kamerkar S, et al. Exosomes facilitate therapeutic targeting of oncogenic KRAS in pancreatic cancer. Nature. 2017; 546:498–503. [PubMed: 28607485]
48. György B, et al. Rescue of hearing by gene delivery to inner-ear hair cells using exosome-associated AAV. Mol Ther. 2017; 25:379–391. [PubMed: 28082074]
49. Kim SM, et al. Cancer-derived exosomes as a delivery platform of CRISPR/Cas9 confer cancer cell tropism-dependent targeting. J Control Release. 2017; 266:8–16. [PubMed: 28916446]
50. Wang Q, et al. ARMMs as a versatile platform for intracellular delivery of macromolecules. Nat Commun. 2018; 9:960. [PubMed: 29511190]
51. Hood JL, Scott MJ, Wickline SA. Maximizing exosomes colloidal stability following electroporation. Anal Biochem. 2014; 448:41–49. [PubMed: 24333249]
52. Alhasan AH, Patel PC, Choi CHJ, Mirkin CA. Exosome encased spherical nucleic acid gold nanoparticle conjugates as potential microRNA regulation agents. Small. 2014; 10:186–192. [PubMed: 24106176]
53. Busato A, et al. Magnetic resonance imaging of ultrasmall superparamagnetic iron oxide-labeled exosomes from stem cells: a new method to obtain labeled exosomes. Int J Nanomedicine. 2016; 11:2481–2490. [PubMed: 27330291]
54. Illes B, et al. Exosome-Coated Metal–Organic Framework Nanoparticles: An Efficient Drug Delivery Platform. Chem Mater. 2017; 29:8042–8046.
55. Betzer O, et al. In vivo neuroimaging of exosomes using gold Nanoparticles. ACS Nano. 2017; 11:10883–10893. [PubMed: 28960957]
56. Ha D, Yang N, Nadithe V. Exosomes as therapeutic drug carriers and delivery vehicles across biological membranes: current perspectives and future challenges. Acta Pharm Sin B. 2016; 6:287–296. [PubMed: 27471669]
57. Luan X, et al. Engineering exosomes as refined biological nanoplatforms for drug delivery. Acta Pharmacol Sin. 2017; 38:754–763. [PubMed: 28392567]
58. Sebastian V, Smith CD, Jensen KF. Shape-controlled continuous synthesis of metal nanostructures. Nanoscale. 2016; 8:7534–7543. [PubMed: 26927867]
59. Herrer L, et al. High surface coverage of a self-assembled monolayer by in situ synthesis of palladium nanodeposits. Nanoscale. 2017; 9:13281–13290. [PubMed: 28858363]
60. Zhang D, et al. An In situ TEM study of the surface oxidation of palladium nanocrystals assisted by electron irradiation. Nanoscale. 2017; 9:6327–6333. [PubMed: 28230871]
61. Kikot P, Polat A, Achilli E, Fernandez Lahore M, Grasselli M. Immobilized palladium(II) ion affinity chromatography for recovery of recombinant proteins with peptide tags containing histidine and cysteine. J Mol Recognit. 2014; 27:659–668. [PubMed: 25277090]
62. Raedler LA. Farydak (Panobinostat): First HDAC Inhibitor Approved for Patients with Relapsed Multiple Myeloma. Am Health Drug Benefits. 2016; 9:84–87.
63. Zheng S, et al. Biocompatible Boron-Containing Prodrugs of Belinostat for the Potential Treatment of Solid Tumors. ACS Med Chem Lett. 2018; 9:149–154. [PubMed: 29456804]
64. Rubio-Ruiz B, Weiss JT, Unciti-Broceta A. Efficient palladium-triggered release of vorinostat from a bioorthogonal precursor. J Med Chem. 2016; 59:9974–9980. [PubMed: 27786474]
65. Wang H, et al. Discovery of (2E)-3-{2-Butyl-1-[2-(diethylamino)ethyl]-1H-benzimidazol-5-yl}-N-hydroxyacrylamide (SB939), an Orally Active Histone Deacetylase Inhibitor with a Superior Preclinical Profile. J Med Chem. 2011; 54:4694–4720. [PubMed: 21634430]
66. Sancho-Albero M, et al. Exosome origin determines cell targeting and the transfer of therapeutic nanoparticles towards target cells. J Nanobiotechnol. 2019; 17:16.
67. Sletten EM, Bertozzi CR. Bioorthogonal chemistry: fishing for selectivity in a sea of functionality. Angew Chem Int Ed. 2009; 48:6974–6998.
68. Li J, Chen PR. Development and application of bond cleavage reactions in bioorthogonal chemistry. Nat Chem Biol. 2016; 12:129–137. [PubMed: 26881764]

69. Devaraj NK. The Future of Bioorthogonal Chemistry. ACS Cent Sci. 2018; 4:952–959. [PubMed: 30159392]

Europe PMC Funders Author Manuscripts

Europe PMC Funders Author Manuscripts

Europe PMC Funders Author Manuscripts

Europe PMC Funders Author Manuscripts

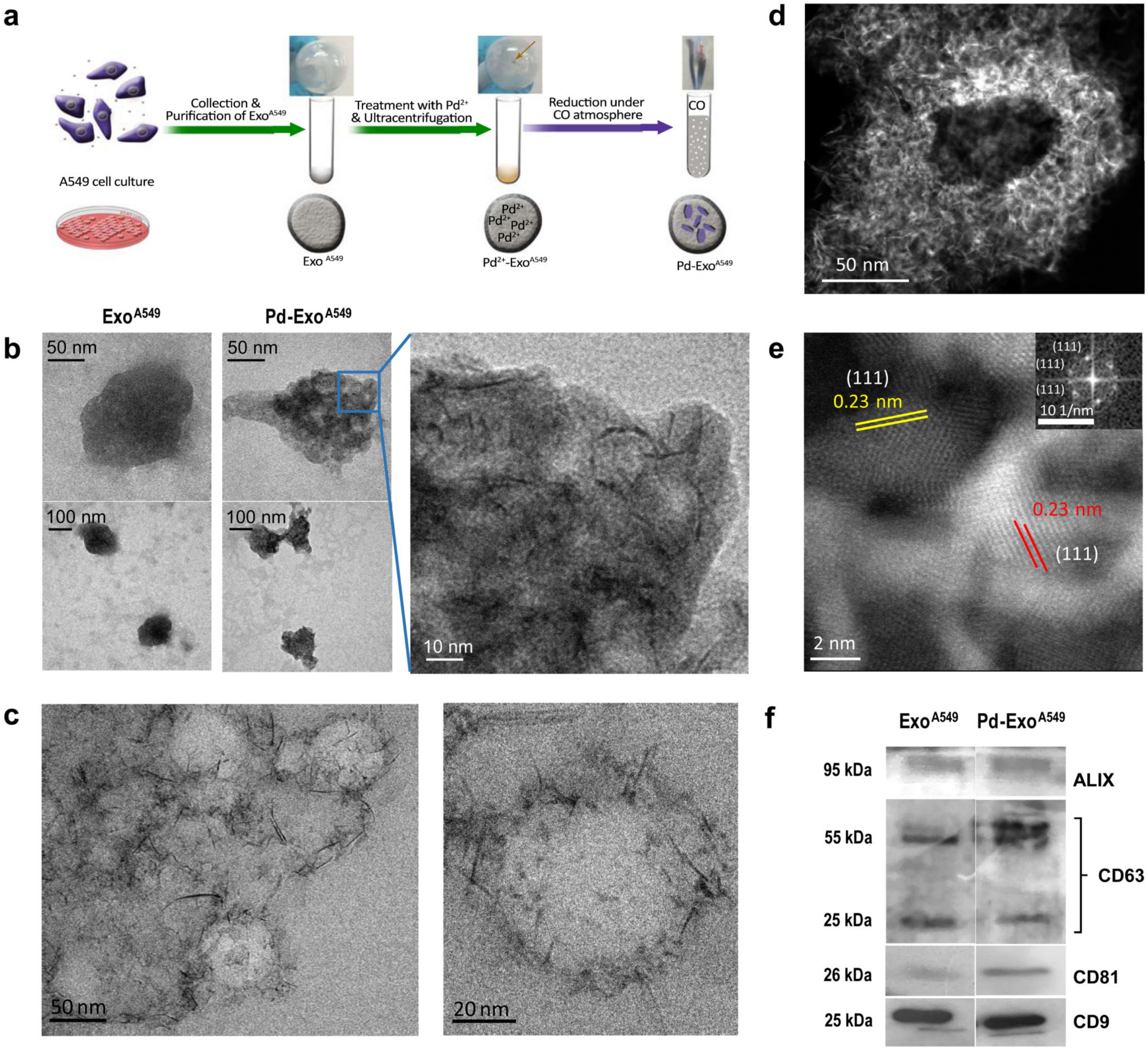

**Figure 1. Preparation and characterization of Pd-functionalised exosomes.**

**(a)** Overview of the step-wise protocol to generate **Pd-Exo**$^{\mathbf{A549}}$ from A549 cells. **(b)** Representative TEM images of **Exo**$^{\mathbf{A549}}$ and **Pd-Exo**$^{\mathbf{A549}}$ at different magnifications. **(c)** Representative cryo-TEM images of **Pd-Exo**$^{\mathbf{A549}}$ at two magnifications. **(d)** HRSTEM-HAADF image of a representative **Pd-Exo**$^{\mathbf{A459}}$. **(e)** HRSTEM-HAADF zoomed-in image showing highly-crystalline Pd nanostructures with a lattice spacing of 0.23 nm, which correspond to Pd (1 1 1)-surfaces. Inset shows the FFT spectrum generated from the image. **(f)** Western blots of exosome-specific biomarkers ALIX, CD63, CD81 and CD9 of **Exo**$^{\mathbf{A549}}$ and **Pd-Exo**$^{\mathbf{A549}}$.

Europe PMC Funders Author Manuscripts
Europe PMC Funders Author Manuscripts

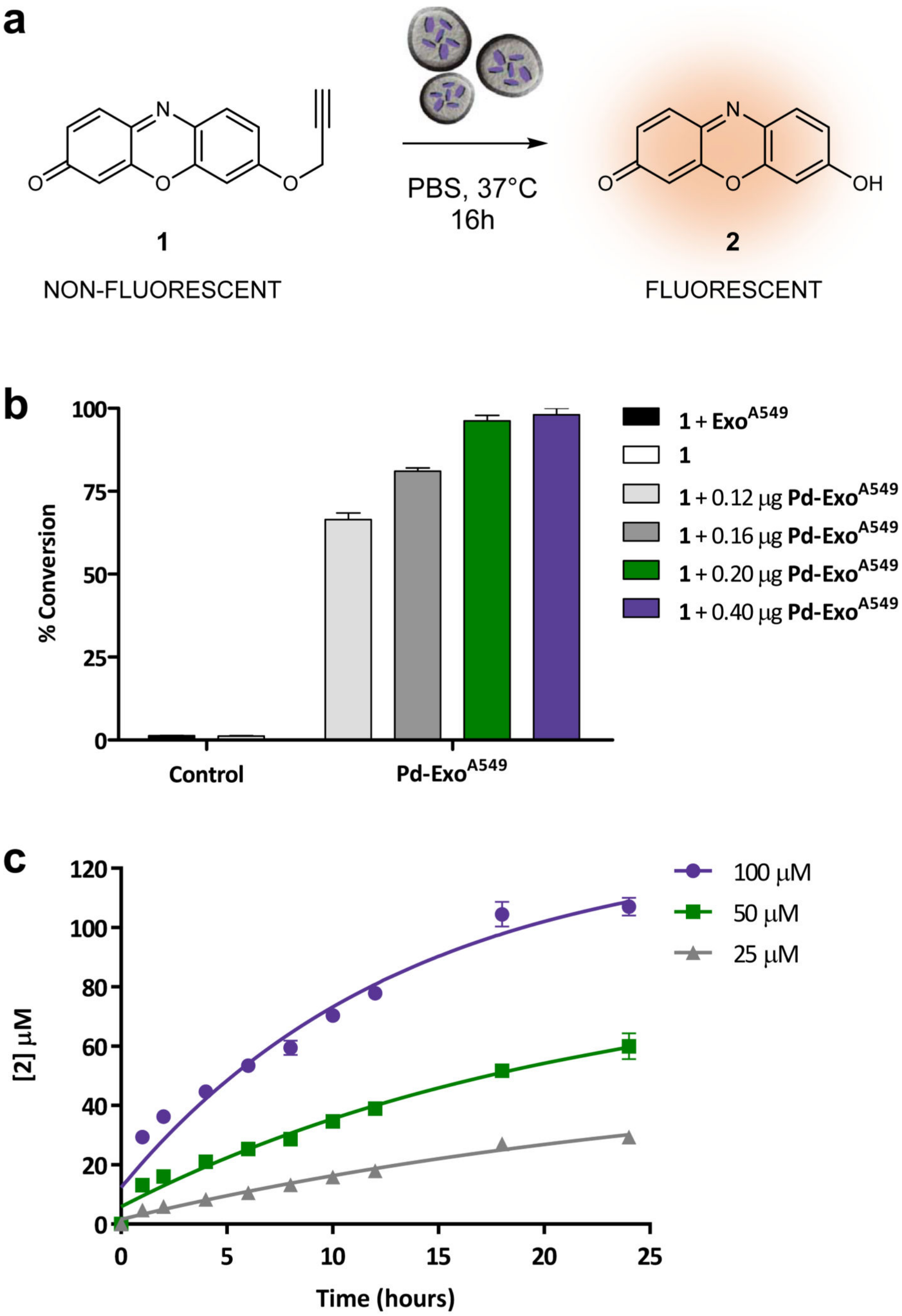

**Figure 2. Study of the catalytic properties of Pd-Exo$^{A549}$.**

**(a)** Conversion of non-fluorescent **1** into highly red-fluorescent resorufin **2** mediated by **Pd-Exo$^{A549}$** under biocompatible conditions (37 °C, PBS, pH 7.4, isotonicity). **(b)** Conversion efficiency after 16 h incubation of **1** (100 µM) with **Pd-Exo$^{A549}$** (0.12, 0.16, 0.2 and 0.4 µg / 100 µL). Conversion values (%) were calculated from fluorescence intensity measurements at $\lambda_{ex/em}$= 540/590 nm using the fluorescence intensity of **2** (100 µM) as 100 %. Negative controls: **1** (100 µM) with or without **Exo$^{A549}$** (0.2 µg/100 µL). Error bars: ±SD, n=3. **(c)** Kinetic study of the reaction of **Pd-Exo$^{A549}$** (0.2 µg/100µL) with different concentrations of

**1** (25, 50 and 100 μM) in PBS at 37 °C. Concentration values of product **2** were calculated from fluorescence intensity measurements at $\lambda_{ex/em}$= 540/590 nm. Curves fit: non-linear exponential equation. Error bars: ±SD, n=3.

Europe PMC Funders Author Manuscripts

Europe PMC Funders Author Manuscripts

Europe PMC Funders Author Manuscripts

Europe PMC Funders Author Manuscripts

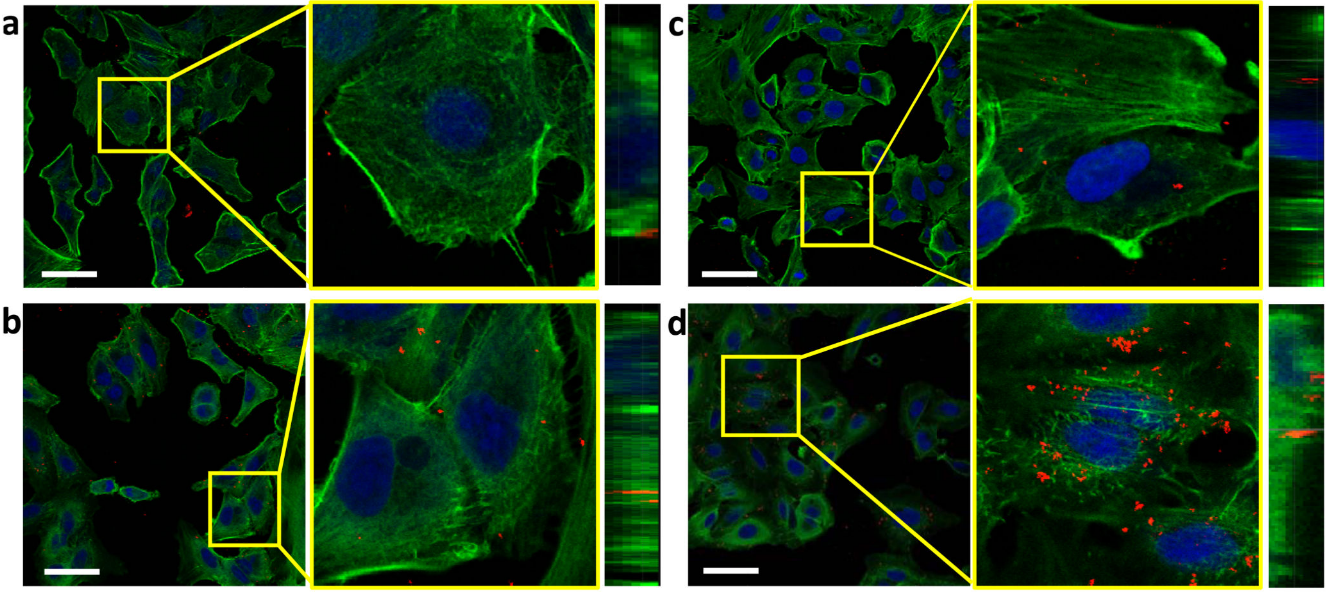

**Figure 3. Confocal study of Pd-Exo$^{A549}$ internalization in A549 cells.**

Merged confocal images of A549 cells after treatment with **Pd-Exo$^{A549}$** for 1 h (**a**), 2 h (**b**), 4 h (**c**) and 6 h (**d**). Actin fibres (phaloidin-488) are shown in green, cell nuclei (Draq5) in blue and clusters of **Pd-Exo$^{A549}$** in red. Scale bar= 50 µm. The middle and right images show the amplified and z-stacks sections, respectively.

Europe PMC Funders Author Manuscripts

Europe PMC Funders Author Manuscripts

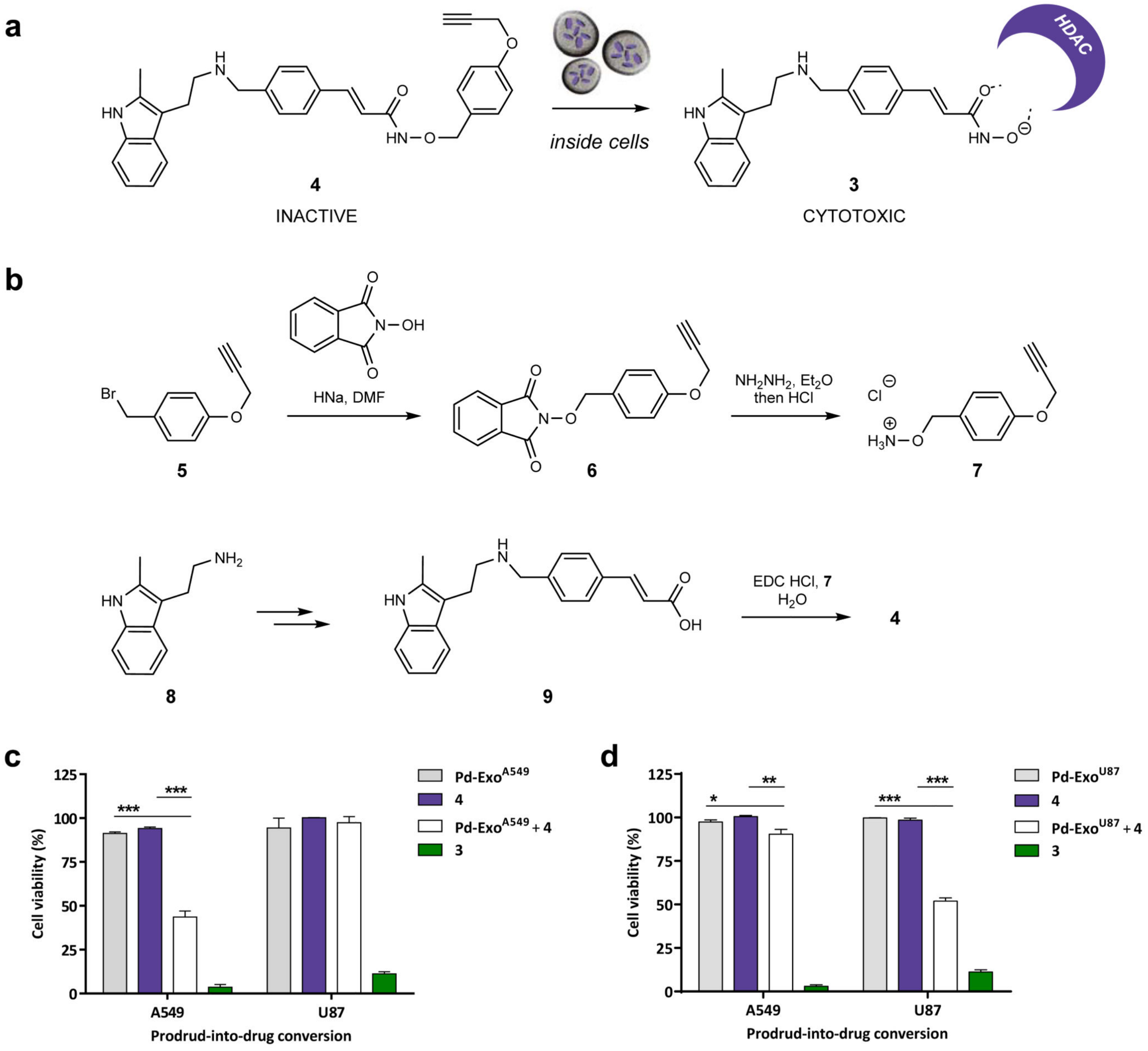

**Figure 4. Design and synthesis of prodrug 4 and targeted intracellular activation mediated by Pd-Exo$^{A549}$ and Pd-Exo$^{U87}$ in A549 and U87 cells.**

**(a)** Intracellular **Pd-Exo$^{A549}$**-mediated conversion of prodrug **4** into clinically-approved HDAC inhibitor **3**. **(b)** Total synthesis of compound **4**. **(c) Pd-Exo$^{A549}$**-mediated uncaging of **4** inside cells. A549 and U87 cells were incubated for 6 h with 0.4 and 0.53 µg / 100 µL, respectively. Cells were thoroughly washed to eliminate extracellular vesicles followed by addition of prodrug **4** (0.2 µM). Controls: **Pd-Exo$^{A549}$** only (–ve control, grey); prodrug **4** only (–ve control, purple); **3** (+ve control, green). Cell viability was measured at day 5 using PrestoBlue. Error bars: ± SEM, n = 3. (**d**) **Pd-Exo$^{U87}$**-mediated uncaging of **4** inside cells. A549 and U87 cells were incubated for 6 h with 0.4 and 0.53 µg / 100 µL, respectively. Cells were thoroughly washed to eliminate extracellular vesicles followed by addition of prodrug

**4** (0.2 µM). Controls: **Pd-Exo$^{\mathbf{U87}}$** only (–ve control, grey); prodrug **4** only (–ve control, purple); **3** (+ve control, green). Cell viability was measured at day 5 using PrestoBlue. Error bars: ± SEM, n = 3.

Europe PMC Funders Author Manuscripts

Europe PMC Funders Author Manuscripts